

UC Santa Barbara

UC Santa Barbara Electronic Theses and Dissertations

Title

Characterizing Groundwater Fluxes in Death Valley, California, using InSAR

Permalink

<https://escholarship.org/uc/item/7n12r58z>

Author

Thacker, Robert Edward

Publication Date

2024

Peer reviewed|Thesis/dissertation

UNIVERSITY OF CALIFORNIA

Santa Barbara

Characterizing Groundwater Fluxes in Death Valley, California, using InSAR

A Thesis submitted in partial satisfaction of the

requirements for the degree of Master of Arts

in Geography

By

Robert Edward Thacker

Committee in charge:

Professor Hugo A. Loaiciga, Chair

Professor Qinghua Ding

Professor Chen Ji

March 2024

The thesis of Robert E. Thacker is approved.

Qinghua Ding

Chen Ji

Hugo A. Loaiciga, Committee Chair

March 2024

Characterizing Groundwater Fluxes in Death Valley, California, using InSAR

Copyright ©2024

By

Robert Edward Thacker

ACKNOWLEDGEMENTS

This work is dedicated to my Wife Vida and my Parents. Thank you for your love and support.

“To those who seek life in the valley of death, may you sense the water beneath your feet, and know that even in the driest air the water will rise in season.” R.E.T. 2024

ABSTRACT

Characterizing Groundwater Fluxes in Death Valley, California using InSAR

By

Robert Edward Thacker

Groundwater is a fundamental resource for humans and represents a major volumetric phase of the terrestrial water cycle. Observations indicate that climate change is altering precipitation patterns globally and inducing an increase in the frequency and magnitude of extreme events. These extreme precipitation events may buffer water resources long-term in the face of increasing droughts by contributing significant recharge to aquifers. Nonetheless, uncertainties remain regarding the influence of local geological variability and the unpredictability of regional weather patterns on extreme precipitation induced groundwater recharge at the catchment scale. This complexity necessitates further exploration and requires both targeted testing and extended observational studies. This study applied interferometric synthetic aperture radar (InSAR) to characterize groundwater fluxes in the ungauged endorheic basin Death Valley, California, from December 2018 through December 2023. Over this period there was mean upward vertical displacement (uplift) of ~1.5 to 2 cm across the basin caused by recharge. T-mode principal component analysis was used to isolate dominant deformation signals coinciding with extreme precipitation events. This study demonstrates the applicability of InSAR as a viable tool to assess

groundwater fluxes in response to precipitation variability, furthering our understanding of terrestrial water cycling in a warming world.

TABLE OF CONTENTS

1. BACKGROUND AND OBJECTIVES	1
1.1 Groundwater and Climate.....	1
1.2 Measuring Groundwater Fluxes – Challenges and Opportunities	4
1.2.1 Aquifer Properties	4
1.2.2 Measurement Techniques and Challenges.....	9
1.3 Objectives and Study Area	14
2. DATA AND METHODS.....	18
2.1 Climatological	18
2.2 GRACE and InSAR	19
2.3 Time Mode (T-Mode) Principal Component Analysis (TPCA)	25
3. RESULTS	27
4. DISCUSSION	34
5. CONCLUSIONS	35
REFERENCES.....	36

1. BACKGROUND AND OBJECTIVES

1.1 Groundwater and Climate

Groundwater is a fundamental resource for humans and many ecosystems, providing a perennial source of high-quality freshwater and sustained baseflow during drought (Alley, 2002). Recently, there has been great interest in understanding the importance of groundwater systems in the context of climate change (Loaiciga, 2003; Loaiciga and Roh, 2024). Climate change directly and indirectly impacts groundwater systems by influencing the spatiotemporal distribution of natural recharge (direct impacts) and influences the behavior of human extraction and land use-changes (indirect impacts) (Taylor et al.(a), 2013). Groundwater currently accounts for ~30% of the total freshwater used by humans (United Nations, 2022). However, demand is likely to increase as global population increases and climate change reduces the availability of other freshwater sources, inducing greater extraction of groundwater (Bierkens and Wada, 2019). Apart from sustaining human populations and natural ecosystems it has been observed that groundwater extraction may be the second leading contributing factor to global mean sea level rise (GMSLR), behind melting of glaciers and sea ice (Seo et al., 2023). GMSLR in turn produces secondary impacts, such as increase in sea water intrusion, further compromising the available quantity and quality of freshwater resources (Loaiciga, 2012). These conditions compel the need to characterize and understand the dynamics of groundwater systems across spatiotemporal scales and variable lithologies of global aquifers. The key information needed to assess these dynamics include enhanced conceptual models of hydrogeologic conditions and accurate measurements of groundwater *recharge* and *discharge*, henceforth referred to as groundwater fluxes.

It is prudent to recognize the volumetric composition and interconnectivity of the hydrosphere when assessing groundwater fluxes. The Earth's saline oceans cover ~71% of the planetary surface and hold ~97% of its water volume. The remaining ~3% of terrestrial water is ~1% saline groundwater and lakes, with the remaining 2% existing as freshwater; 96% of which is contained in ice sheets, glaciers, and snowpacks (Durack, 2015; Abbott et al., 2019). This results in a remaining volume of accessible freshwater of approximately 835,000 km³, which exists as groundwater (630,000 km³) and surface water (205,000 km³) (Abbott et al. 2019). There is great uncertainty regarding our understanding of the rate of exchange and the physical conditions (diffuse vs. focused recharge) facilitating mass exchanges between surface water and groundwater, which means one must focus attention on the relative responses of these storage reservoirs to energetic perturbations at different spatial and temporal scales.

The global hydrologic cycle is a complex system of energy and mass that operates at a wide range of spatiotemporal scales. This cycle is a continuous transfer of liquid, solid, and gaseous phase water through oceanic, atmospheric, cryogenic, and terrestrial reservoirs (Stocker et al., 2013). Global patterns of evaporation and precipitation (the engine) are controlled by the Earth's energy balance (O'Gorman, 2012), and perturbations to this budget are increasingly discussed as increased greenhouse concentrations have induced warmer temperatures (Meinshausen et al, 2017). The relationship between temperature and the water cycle can loosely be explained by the Clausius-Clapeyron equation (see, e.g., Fermi, 1936), which states that water vapor holding capacity increases with air temperature. Thus, the generalized conceptual model in climatology and hydrology is that a warming climate will produce a net increase in atmospheric absolute humidity (Fischer, 2016). This effect has produced substantial observational evidence that extreme precipitation events are occurring

with increasing frequency and magnitude (Myhre et al., 2019). However, it is important to recognize that the definition of ‘extreme precipitation’ is non-standardized, which may affect conclusions concerning the relationship between warmer temperature and precipitation event magnitude (Pendergrass, 2018). In addition, there exists uncertainty in comparing observational data vs model estimates of atmospheric humidity (Simpson et al., 2023).

There is a growing body of literature that explores the relationship between the frequency and magnitude of extreme precipitation events and its effects on groundwater recharge. For example, in semi-arid tropical East Africa, analysis of a 55-year record of in-situ groundwater level measurements and monthly rainfall suggests that groundwater recharge is highly dependent on anomalously intense seasonal rainfall (Taylor et al.(b), 2013). Many drought-prone, semi-arid regions are benefitting from the increased frequency of extreme precipitation events despite overall drier conditions, allowing communities to buffer water resource supplies and mitigate the negative effects of drought (Adloff, 2022). This type of work has enhanced the understanding of how groundwater may buffer water supplies in a warming world, prompting the IPCC 6th assessment report¹ to conclude section 8.3.1.7.4 on groundwater with the following statement: “*There is medium confidence that increased precipitation intensities, partly due to human influence, have enhanced groundwater recharge, most notably in the tropics.*” Nonetheless, uncertainties remain regarding the influence of local geological variability and the unpredictability of regional weather patterns on ‘extreme’ precipitation induced groundwater recharge at the catchment scale (Cuthbert, 2019). This

¹ IPCC, 2021: Climate Change 2021: The Physical Science Basis. Contribution of Working Group I to the Sixth Assessment Report of the Intergovernmental Panel on Climate Change [Masson-Delmotte, V., P. Zhai, A. Pirani, S.L. Connors, C. Péan, S. Berger, N. Caud, Y. Chen, L. Goldfarb, M.I. Gomis, M. Huang, K. Leitzell, E. Lonnoy, J.B.R. Matthews, T.K. Maycock, T. Waterfield, O. Yelekçi, R. Yu, and B. Zhou (eds.)]. Cambridge University Press, Cambridge, United Kingdom and New York, NY, USA, 2391 pp. doi: <https://doi.org/10.1017/9781009157896>

complexity necessitates further exploration and requires both targeted testing and extended observational studies.

The objectives of this work are to (1) explore the capacity of interferometric synthetic aperture radar (InSAR) to characterize groundwater fluxes in Death Valley, CA, and (2) relate these InSAR measurements to extreme precipitation events. Death Valley offers a unique natural laboratory as an endorheic basin (i.e., a basin without drainage to a sea or lake) to explore the effects of extreme precipitation events on observable signals of groundwater fluxes that are decoupled from anthropogenic distortion i.e. groundwater pumping.

1.2 Measuring Groundwater Fluxes – Challenges and Opportunities

It is useful to technically define the parameters that govern this process to accurately characterize groundwater fluxes in response to a warming world. The subsequent sections describe (1) the physical properties of aquifers and the measurable processes associated with groundwater fluxes, and (2) available measurement techniques and associated challenges.

1.2.1 Aquifer Properties

Groundwater flow is a thermodynamic process, and the forces acting upon groundwater include gravity, external pressure, and molecular attraction i.e. shearing resistance/viscosity (Fetter, 2001). Measurements of hydraulic head (h) represent the total mechanical energy per unit weight of groundwater and is described by the following equation:

$$h = z + \frac{P}{\rho g} \quad (1)$$

where z , P , ρ , g and denote respectively the elevation of the center of gravity of the fluid above a reference elevation, the fluid pressure, the density of water, and the acceleration of

gravity. Given that aquifers are a 3-dimensional diffusive media, the distribution of hydraulic head across an aquifer can be described using equipotential surfaces. The distribution of this network constitutes the hydraulic gradient. Aquifers are dynamic and respond to both external (recharge) and internal (discharge) fluxes which can be observed as changes in hydraulic head and storage (Castellazzi, 2016). Storage change (ΔS), is a key metric for quantifying groundwater fluxes and can be computed for a time-averaged scenario using the following equation:

$$\overline{\Delta S} = \overline{R} - \overline{D} - \overline{E} - \overline{Q} \quad (2)$$

in which \overline{R} , \overline{D} , \overline{E} , \overline{Q} , denote respectively recharge entering the aquifer storage through natural (percolation) or artificial means, the discharge to adjacent aquifers, rivers, lakes, springs, wetlands, or ocean, the discharge fluxes of evapotranspiration, and the fluxes from groundwater pumping (Loaiciga, 2017). In many cases, at least one or all of these fluxes are difficult to estimate due to the complexities inherent to these processes. It is therefore not uncommon to estimate (ΔS) from measurements of hydraulic head change (Δh) at wells across a basin over a specified interval. Considering vertical heterogeneities, the following equation describes this relationship across aquifer layers for a specified period:

$$\Delta S_t = \sum_{k=1}^K S_{ck} * \Delta h_{tk} * A_k \quad (k = 1, 2, \dots, K); (t = 1, 2, \dots, N) \quad (3)$$

in which Δh_{tk} , A_k , S_{ck} denote respectively the change in hydraulic head across the basin in the specified time interval within layer k , the plan-view area of layer k , and the storativity of layer k (Loaiciga, 2017). Storativity (S_c) is a dimensionless value defined as the volume of water that is released from storage per unit surface area of the aquifer per unit decline in hydraulic head (Fetter, 2001).

For *confined* aquifer conditions this is defined as follows:

$$S_c = b (\rho g(\alpha + n \beta)) \quad (4)$$

where S_c , b , ρ , g , α , n , β , denote respectively the confined aquifer storativity, aquifer thickness, the density of water, the gravitational acceleration, the compressibility of aquifer sediments, the total porosity (volume of voids/total volume), and the compressibility water (Freeze and Cherry, 1979). These terms collectively constitute an additional coefficient known as specific storage ($S_s = \rho g(\alpha + n\beta)$), which represents “the volume of water per unit volume of saturated aquifer that is stored or expelled from storage owing to compressibility of the mineral skeleton and the pore water per unit change in hydraulic head” (Fetter, 2001). This term is of particular interest when exploring methods to characterize groundwater fluxes. For *unconfined* aquifer conditions, (S_c) is defined as:

$$S_{c(unconfined)} = b * S_s + S_y \quad (5)$$

where only one additional parameter is introduced, S_y which is the aquifer specific yield, defined as the ratio of the volume of water that drains from a volume of aquifer due to gravity (Fetter, 2001). S_y , or drainage porosity, may also be referred to as unconfined storativity (Castellazzi, 2016). The distinction between confined and unconfined conditions is relevant to characterizing groundwater fluxes because values of S_c can range from 5×10^{-5} to 5×10^{-3} for confined aquifers (Todd, 1980) and 0.1 to 0.3 for unconfined aquifers (Lohman, 1972). This implies that in confined aquifers, the storage change (ΔS) necessary to accommodate groundwater fluxes is constrained by the *elastic* properties of the aquifer and confining layer (aquitar) sediment and expansion of water (Ingebritsen et al., 2006). When confined systems are pumped or receive recharge, water is released or gained from storage via elastic

deformation (compression and expansion). Whereas in unconfined aquifers, storage change (ΔS) is governed by S_y , reflecting a broader volume of aquifer sediment participating in water storage and movement. In unconfined systems $b * S_s < S_y$ and $S_c \cong S_y$ (Lohman, 1972).

Hydraulic head (h) (eq.1) is directly measurable from a well or piezometer, whereas storativity (S_c), specific storage (S_s), and specific yield (S_y) are usually derived by conducting aquifer pumping tests which utilize empirically derived mathematical relationships (e.g., Theis, 1935) that relate aquifer drawdown to aquifer properties in response to an applied stress (Loaiciga, 2009). However, storage changes (ΔS) within an aquifer can induce an additional observable phenomenon apart from changes in hydraulic head which relate to the specific storage (S_s), and that is ground surface deformation. Local storage changes (ΔS) induce changes in aquifer pore pressure by increasing or decreasing vertical effective stress, causing expansion or reduction of pore volume, resulting ground surface deformation (Ingebritsen et al., 2006; Loaiciga, 2013; Galloway & Burbey, 2011). This deformation can be elastic or inelastic. Inelastic deformation, or land subsidence, occurs when a stress applied (usually induced by aquifer pumping) to aquifer sediments reduces the void or pore volume leading to a permanent loss of porosity and permeability. Elastic deformation is governed by the elastic properties of aquifer sediments and occurs when aquifer sediments temporarily compress or expand in response to the applied stress (Domenico and Schwartz, 1998). This process can be understood by applying the (1D) principle of effective stress first outlined by Terzaghi (Terzaghi, 1925) which is described by the following equation for cases of constant total stress:

$$\Delta\sigma_e = -\rho g \Delta h \quad (6)$$

in which $\Delta\sigma_e$, ρ , g , Δh , denote respectively the vertical effective stress, the density of water, the acceleration of gravity, and the hydraulic head change. These variables collectively represent changes in interstitial fluid pressure ($\Delta P = \rho g \Delta h$). However, this commonly utilized framework is for ideal scenarios where it is assumed that an instantaneous vertical load is applied to the soil causing instantaneous increase in vertical total stress. It is important to reconcile the assumptions of this model with the properties of groundwater flow and test this model under various scenarios of groundwater flow and sediment properties (Loaiciga, 2013). For example, during groundwater pumping and potentially during recharge, the applied pressure incrementally increases or decreases gradually, creating a gradient of pressure towards steady state (Loaiciga, 2013). Another often overlooked detail is the evaluation of vertical effective stresses relative to unconfined or confined groundwater flow regimes previously discussed. There exists a need to evaluate these principles not only for specific pumping regimes or increases in vertical effective stress, but for decreased vertical effective stress induced by groundwater recharge. In addition, the compressibility of aquifer sediments is the fundamental control when relating surface displacement to changes in aquifer pore pressure. For comparison purposes, the following describes the range of compressibility of aquifer material (Freeze and Cherry, 1979):

Table 1. Range of compressibility ty corresponding to soil and rock.

Material	Compressibility (α) $\left(\frac{m^2}{N}\right)$
Clay	10^{-8} to 10^{-6}
Sand	10^{-9} to 10^{-7}
Gravel	10^{-10} to 10^{-8}
Jointed Rock	10^{-10} to 10^{-8}
Sound Rock	10^{-11} to 10^{-9}

The general paucity of detailed 3D conceptual models of the distribution of aquifer sediments inhibits the ability to accurately relate the groundwater fluxes to vertical ground movement. However, if the distribution of sediments within an aquifer is known to some degree, one might attribute the mechanisms of surface deformation, or lack thereof, to the compressible nature of the aquifer sediments. For example, the widely accepted conceptual model of land subsidence in the southern Central Valley of California, is attributed to a large clay layer known as the Corcoran clay. It is assumed that this layer regulates the inelastic compaction of the aquifer sediments in response to pumping (Lees et al. 2021). However, even if advanced conceptual models of aquifer sediments are absent, measurements of ground surface deformation can provide first-order, general insights on aquifer mechanics and seasonal behavior of groundwater fluxes (Galloway and Hoffmann, 2007).

1.2.2 Measurement Techniques and Challenges

The previous section describes aquifer properties and provides an understanding of how aquifers respond to groundwater fluxes. It should be noted that groundwater age (isotope analysis), chemical composition, and groundwater temperature may also provide insight into

the nature of groundwater fluxes but are not considered in this study (Jasechko, 2019). Having defined the technical parameters associated with groundwater fluxes, the subsequent sections outline the traditional and emerging measurement methods and associated challenges of quantifying groundwater fluxes.

The traditional method used to observe groundwater fluxes consists of directly measuring the hydraulic head (h) (eq.1) within a well, which can be achieved using a suite of instruments that include electronic sounders, chalk tapes, pressure transducers, sonar equipment, or air pressure gauges (Taylor and Alley, 2001). In a management scenario, measurements of hydraulic head are compared across wells within a basin to infer the spatiotemporal variability of the potentiometric surface within an aquifer, which can be used to (1) determine safe yield or other sustainability metrics, (2) estimate total storage changes (3) provide calibration data for groundwater flow models, (4) manage land subsidence or undesirable surface deformation, (5) interpret groundwater-surface water interactions, (6) interpret groundwater quality data, (7) assess the effectiveness of groundwater recharge projects and variability of natural recharge, and (8) assess health of riparian habitat, among other key considerations (Wildermuth Environmental Inc., 2019). In addition to these regional applications, global analyses of available groundwater level data can be used to understand global dynamics of groundwater fluxes (Jasechko and Perrone, 2021). However, despite the effectiveness of these traditional methods of measuring groundwater fluxes, many basins lack a spatially coherent monitoring network of wells, introducing uncertainty to the analyses associated with these objectives. Recent studies have highlighted this, noting that despite the compilation and analysis of the most comprehensive global data set of groundwater level data to date, limitations of the global spatiotemporal coverage of these data exist, and inhibit

characterizations of groundwater fluxes in many regions (Jasechko et al., 2024). This limitation necessitates the exploration of additional tools to augment traditional methods, and thus enhance our ability to characterize groundwater fluxes from local, regional, and global scales in relation to a warming world. Two remote sensing techniques have emerged as viable approaches to achieve this: GRACE and InSAR. The subsequent section will outline the current state of science with regards to these technologies.

GRACE

The Gravity Recovery and Climate Experiment (GRACE) mission was jointly launched in March 2002 by NASA and the German Aerospace Center (DLR) with the objective of monitoring spatiotemporal changes of Earth's gravity field (Tapley, 2004). This initial mission was decommissioned in November 2017 and replaced by the GRACE Follow-On (GRACE-FO) mission which was launched in May 2018 (Chen et al, 2021). The GRACE system consists of twin satellites separated at a distance (along-track) of ~200 km orbiting Earth at an altitude of ~500 km and 89.5° inclination. GRACE measures changes in Earth's gravity field by tracking changes to inter-satellite range at micro-meter resolution (Chen et al., 2018). This allows for the detection of ~1 cm in water thickness equivalent (WTE) distributed across an area equivalent to the altitude of the satellite pair and has resulted in the ability to monitor global total water storage (TWS) changes (Chen, 2018). The advantage of using gravimetric techniques to track hydrologic fluxes is that gravity anomalies are a direct measurement of mass change independent of aquifer lithology and represent a vertical integration of all water storage components (Li et al, 2019).

It is possible to isolate groundwater storage changes by using a water balance approach:

$$\Delta GWS = \Delta TWS - (\Delta SWS + \Delta SMS + \Delta SIS) \quad (7)$$

where ΔGWS , ΔTWS , ΔSWS , ΔSMS , and ΔSIS , denote respectively the change in groundwater storage, the change in total water storage measured by GRACE, the change in surface water storage, the change in soil moisture storage, and the change in snow and ice water storage (Castellazzi, 2016). Thus, the impediment to relating GRACE TWS to any one of these hydrologic reservoirs is the availability of data to estimate each component in the water balance, and as previously discussed, groundwater storage estimates are usually constrained by the availability of hydraulic head measured at wells (Ahamed et al., 2021). However, in dry regions such as Death Valley, California, there is likely to be less noise in (TWS) estimates introduced by SWS and SIS, allowing for greater certainty relating groundwater storage change to GRACE TWS. Another impediment using GRACE TWS data is that the maximum mass field resolution is ~400 km, which limits the interpretation of ΔTWS to basins of an area of ~200,000 km² (Scanlon et al., 2012). Nonetheless, GRACE TWS data provide a powerful tool for the calibration and interpretation of other data sources. For example, it has been demonstrated that GRACE TWS and InSAR data can be used in tandem to monitor hydrologic variation within the Tulare Basin, California (Vasco et al., 2021). This study attempts to leverage this potential and apply the interpretive power of GRACE in reconciling observations of precipitation variability and ground surface deformation in Death Valley.

InSAR

The history and use of synthetic aperture radar (SAR) interferometry is complex and extensive. SAR works by emitting and measuring the return of pulses of energy in the microwave spectrum (300 MHz to 300 GHz) to infer dielectric and physical characteristics of the Earth surface (Simons, 2015). The first interferometric synthetic aperture radar (InSAR) map was used to characterize strain and deformation of an Antarctic ice sheet (Goldstein et al., 1993). Since then, InSAR has been used in a number of applications characterizing processes of deformation occurring on Earth's surface (Smith, 2002). In hydrogeology, it has assisted with the characterization of lithostratigraphic boundaries and aquifer system heterogeneity, the estimation of hydromechanical properties, and the calibration of numerical flow models (Galloway and Hoffmann, 2007). The interferometric processing technique compares the phase difference between multiple synthetic aperture radar (SAR) images taken at different times to detect and measure minute changes in the Earth's surface to millimeter-level precision (Ferretti et al., 2007). The relationship between this phase difference and topographic change can be described by the following equation:

$$H_t = \frac{-\lambda R_1 \sin \theta}{4\pi B_p} \Delta\phi \quad (8)$$

in which H_t , λ , R_1 , θ , B_p , $\Delta\phi$ denote respectively the topographic height, the wavelength of the radar signal, the radar-target distance, the satellite viewing angle, the perpendicular baseline, and the phase difference between 2 SAR acquisitions (Ferretti et al., 2007). Many studies have successfully used InSAR to relate groundwater pumping to land subsidence (see, e.g., Amelung et al., 1999; Riel et al., 2018; Smith et al., 2019), establish the relationship between local irrigation water demand and surface displacement (Levy et al, 2020), and

estimate groundwater recharge and flow regimes (Neely et al., 2021). While many studies focus on measuring the surface deformation in response to groundwater pumping \bar{Q} (eq.2), this study attempts to contribute to the understanding of ground surface deformation in response to natural recharge \bar{R} (eq.2) in a setting devoid of groundwater pumping. The previous sections outline the reality that there is no proverbial silver bullet to accurately estimate groundwater fluxes at regional and global scales. However, given the exponential increase in the power and availability of computation and data, our understanding of groundwater fluxes will expand if these traditional and novel techniques are combined and used in a synergistic way.

1.3 Objectives and Study Area

Geologic Setting

Death Valley National Park is located in eastern California within the western edge of the Basin and Range tectonic province of the western United States. The Basin and Range province is the result of crustal extension that has occurred over the span of tens to millions of years (Glazner et al., 2022). This crustal extension results in normal faulting of the low permeability early to middle Proterozoic crystalline and late Proterozoic siliciclastic basement rocks (Hunt and Mabley, 1966) (Figure 1c). The edges of these tilted blocks form the ridges of the Cottonwood and Panamint Mountains which bound Death Valley to the west, and the Amargosa, Funeral, and Black Mountains to the east (Figure 1b). The valley, or trough, is classified as a pull-apart (extensional) basin that was formed by a large bend in a NW-SE trending strike-slip fault (Figure 1c). This fault action has created the lowest elevation point in North America, Badwater Basin, which lies at an elevation of -282 ft below mean sea level (Glazner et al., 2022). This strike-slip system also acts as a major barrier to groundwater flow along the Black and Amargosa Mountains, inhibiting regional groundwater flow from entering

the valley (Bedinger and Harrill, 2012). In addition to these major fault systems, Death Valley has a complex network of smaller faulting which includes thrust faults, normal faults, and chaos faulting (Bedinger and Harrell, 2012). The Death Valley trough is composed of Tertiary to Quaternary salt and clay intermixed with coarser grained sands and gravels and ranges in depth from 4,000 ft near Artists Drive to 9,000 ft at Badwater Basin (Hunt and Mabley, 1966). The edges of the trough consist of coarse grain sand and gravel alluvial fan deposits. The normal faulting creates a geometry whereby the unconsolidated valley sediments near the interface of the Black Mountains are deeper with smaller alluvial fans. On the western side of the valley at the Panamint Mountain interface, the alluvial fans are spread widely and collectively form a desert feature called 'bajada' that gently slopes east. (Figure 1d). The bajada to the west and the smaller alluvial fans to the east are likely conduits of groundwater recharge during storm events (Belcher et al., 2017). The composition at the surface of Death Valley varies from sand dunes to clay and mud. The surface of Badwater Basin is a salt flat, or salt pan composed of halite with a thickness of ~3-5 feet.

Hydrologic Conditions

Death Valley is bisected by the ephemeral Amargosa River. A number of springs in the Valley along fault zones produce perennial flow and are sourced from the regional groundwater flow system. During the Pleistocene many of the basins within the Basin and Range province were inundated with water, forming extensive lake networks. Death Valley experienced periodic inundation throughout these glacial periods for ~1 million years (Hunt et al., 1966). Pluvial Lake Manley is the most recent incarnation of these ancient lakes with the most recent high stand of the lake occurring ~150,000 years ago during the Tahoe Glaciation. It is estimated that during this high stand, Lake Manley extended 100 miles and had a depth of 600 ft (Glazner

and Sylvester, 2022). Given the elevation of Death Valley, these periods represent regional hydrologic base-level fluctuations. As an endoreic or closed basin, Death Valley can be conceptualized as a “bathtub without a drain” (Glazner and Sylvester, 2022), and receives inflow from the regional system of surface water and groundwater. During inundation, the only way for water to leave the system is through evapotranspiration \bar{E} (eq.2). Understanding the mechanisms controlling groundwater fluxes in Death Valley represents an opportunity to understand terrestrial water cycling at a regional scale and evaluate base-level responses to extreme precipitation events. These dynamics are playing out in real time, with recent storms inducing a return of Lake Manley, albeit at a much smaller scale². The relative contributions of upwelling groundwater from local and regional sources vs. surface water to the formation of Lake Manley is unknown. Thus, exploring techniques to characterize the contribution of groundwater fluxes to these base-level changes may provide a better understanding of groundwater recharge dynamics in arid regions in a warming world. This exploratory study aims to evaluate climatological trends and compare this with variation in total water storage (TWS) data from GRACE and surface displacement measurements derived from InSAR to infer the impact of extreme precipitation on groundwater fluxes.

² <https://www.nps.gov/deva/learn/news/water-levels-are-lower-in-lake-manly.htm>

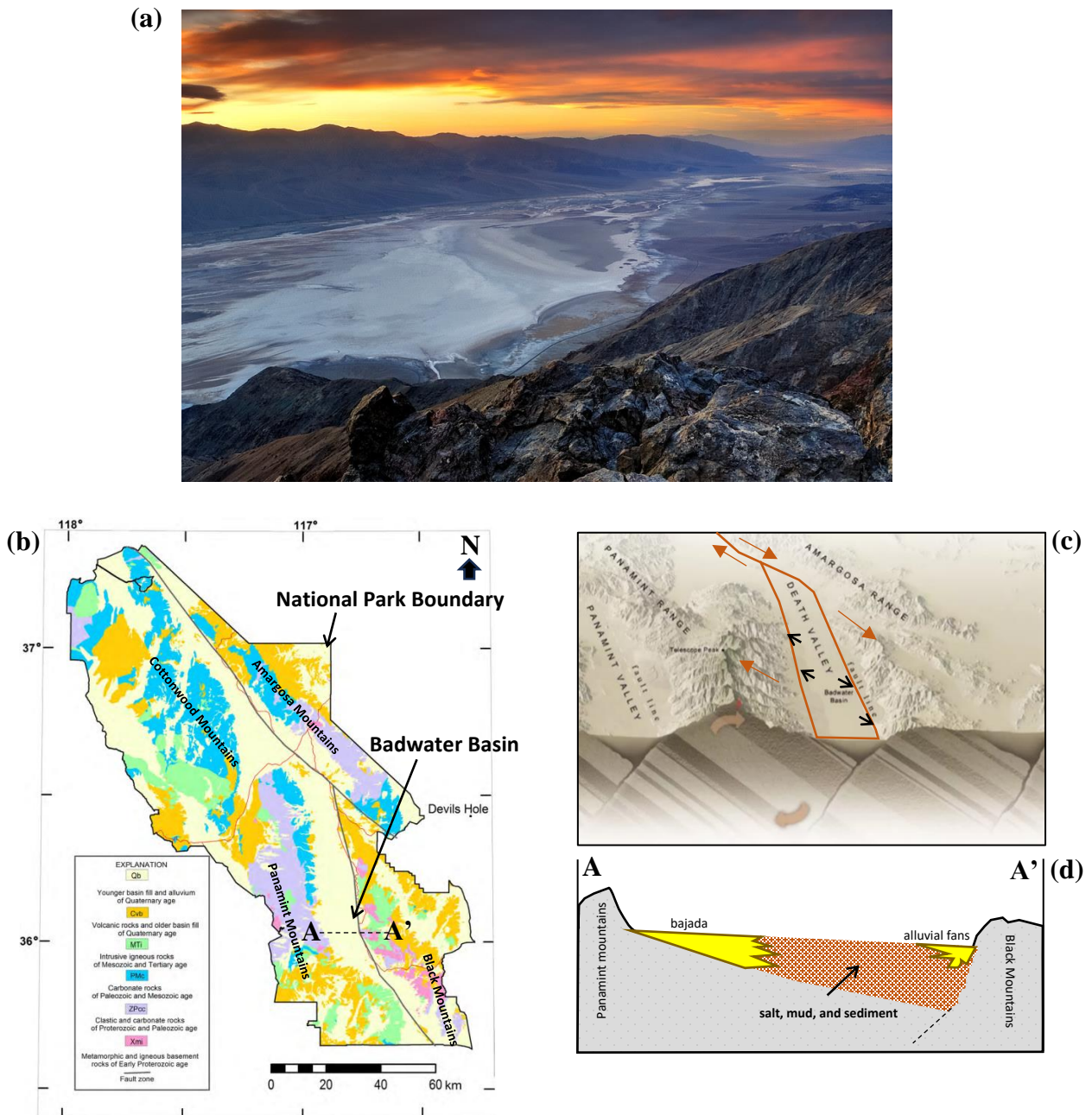


Figure 1: Hydrogeologic setting of Death Valley. (a) Badwater Basin from Dantes View. Note the heterogeneity on the surface of the sediments and salt pan. Photo credit: Andrew Mace, 2009; (b) generalized geologic map of Death Valley adapted from Bedinger and Harrell, 2012. (c) The Death Valley trough is the result of extensional forces resulting from regional normal and strike-slip faulting. The base figure was adapted from the U.S. National Park Service³. (d) Conceptual cross-section diagram of the unconsolidated valley fill from A to A'.

³ <https://www.nps.gov/deva/learn/nature/faults.htm>

2. DATA AND METHODS

2.1 Climatological

Daily precipitation (inch) and maximum and minimum temperature (F^0) data were downloaded and compiled from the National Oceanic and Atmospheric Administration (NOAA) National Centers for Environmental Information database⁴ for the period 4/26/1961 to 12/10/2023. The daily measurements were recorded at the Death Valley National Park Furnace Creek GHCND station (network ID: *GHCND:USC00042319*). There were 2 time periods evaluated for this study 1961-2023 and 2003 to 2023. To characterize long-term climatological trends, the period 1961-2023 was segmented into a 30-year baseline period from 1961-1991 and a subsequent comparison period from 1991-2023. The availability of GRACE TWS data beginning in 2003 informed the decision to assess the period 2003-2023 separately. Given the arid conditions of Death Valley and the occurrence of extreme daily precipitation events, a temporal interval of daily and monthly measurements was selected for this analysis. The cumulative difference from the mean of the analysis period was computed using the following equation to compare and evaluate the occurrence and magnitude of relative wet and dry periods:

$$CDFM = \sum_{i=1}^n (P_i - \bar{P}) \quad (9)$$

where P_i denotes the daily precipitation for the n th day and \bar{P} represents the average daily precipitation value for the period 1961 to 2023 and 2003 to 2023. Positive sloping segments of the CDFM curve indicate wet periods, or periods with above average precipitation and

⁴ <https://www.ncei.noaa.gov/cdo-web/datasets/GHCND/stations/GHCND:USC00042319/detail>

negative sloping segments are indicative of dry periods with below average precipitation. A frequency analysis was conducted for ‘wet days’, or days with measured precipitation to identify the <90th, 90th, 95th, 97th, 98th, and 99th percentile daily events to evaluate the frequency and magnitude of daily precipitation events from 1961-2023. Exceedance probabilities for daily precipitation amounts were computed for the baseline and comparison periods to evaluate the variability and magnitude of daily events over time. This approach is commonly used in flood frequency analysis to calculate recurrence intervals of a particular peak flow discharge. Exceedance probabilities were computed using the following formula for plotting positions:

$$exceedance\ probability\ (\%) = \frac{100 * rank}{n + 1} \quad (10)$$

in which n denotes the number of data values, and $rank$ represents the position of a data value when the sample of values is sorted in decreasing order (i.e., rank = 1 represents the largest sample value). Daily average surface temperature anomalies relative to daily temperature normals (average temperature for a specific day across the baseline period) for the baseline period 1961-1991 were computed to assess the variability of average daily temperatures over the period (1961-2023).

2.2 GRACE and InSAR

GRACE

Terrestrial water equivalent thickness data computed with the Center for Space Research at University of Texas at Austin RL06.2 mascon solutions (Save et al., 2016) were acquired from the JPL GRACE-FO Data Analysis tool⁵ for the mascon with spatial coverage

⁵ <https://grace.jpl.nasa.gov/data/data-analysis-tool/>

over Death Valley over the period 2003 to 2023. The CSR RL06.2 solutions represent a monthly time series of mass anomalies. The mascons have an average width of ~120 km and have a spatial resolution of 0.5 x 0.5 degrees.

InSAR

Synthetic aperture radar (SAR) data from the Sentinel-1 program run by the European Space Agency (ESA) was acquired from the NASA Earth Data, Alaska Satellite Facility Distributed Active Archive Center (ASF DAAC) using the vertex data tool⁶. Sentinel-1 data was used because the data products are designed for analysis of surface deformation using InSAR, and offer global coverage (Sentinel-1 ESA, 2012). The small baseline subset (SBAS) InSAR time series approach was selected for this analysis because SBAS allows for the minimization of decorrelation effects caused by atmospheric disturbances and surface/topographic variation (Berardino et al., 2002). The selection of spatial and temporal thresholds, i.e. perpendicular and temporal baselines, ensure that surface deformation estimates are accurate and reliable. Selecting SAR acquisition pairs with small spatial separation and appropriate temporal intervals associated with the process of interest (aquifer deformation) ensures the quality and accuracy of the interferometric phase signal (Ferretti et al., 2007).

A reference SAR acquisition was selected with geographic coverage over Death Valley and was used to construct a small baseline subset (SBAS) time series of SAR acquisitions within the extent of interest, forming a network of potential SAR pairs to be used in the InSAR analysis. A perpendicular baseline of 220 meters and a temporal baseline of 24 days was selected for the period December 30, 2018, to December 10, 2023, resulting in 705 SAR pairs

⁶ <https://search.asf.alaska.edu/#/>

across 222 scenes and 3 SAR frames (113,114, and 115). While the initial SBAS time series included the period from 2014-2018, the density of SAR scenes did not meet the perpendicular and temporal baseline criteria and were thus excluded from analysis. In addition, the period of analysis from 2018-2023 corresponds to a prolonged dry period within Death Valley punctuated by pulses of extreme precipitation, providing ideal requisite conditions to observe recharge induced deformation. Figure 2 depicts the SBAS time series used in this study. Note that the density of the SBAS network decreases after December 23, 2021, due to instrument electronics failure on the Sentinel-1B satellite⁷.

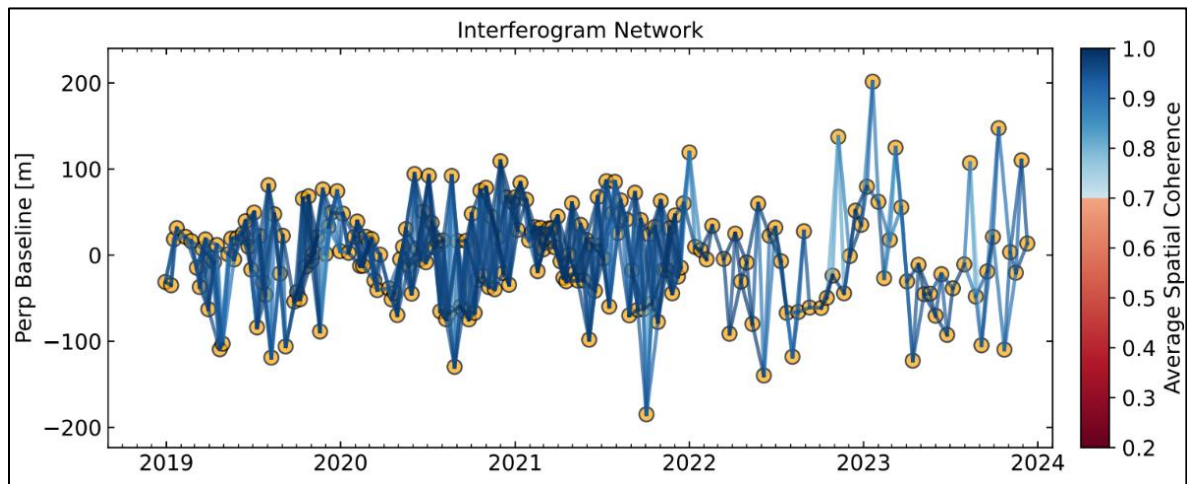


Figure 2: Small baseline subset (SBAS) time-series (interferogram network) and average spatial coherence of SAR pairs for the period December 30, 2018 through December 10, 2023 over Death Valley. Each point (yellow dot) represents a Sentinel-1 SAR acquisition. The blue lines represent the potential SAR ‘pair’ within the specified temporal and perpendicular baselines that are used to compute interferogram data stacks. In addition, the blue lines are weighted by average spatial coherence. The SBAS time series over Death Valley has high average spatial coherence (>0.8) across SAR scenes, indicating that phase differences correspond to ground surface deformation over the period of analysis.

⁷https://www.esa.int/Applications/Observing_the_Earth/Copernicus/Sentinel-1/Mission_ends_for_Copernicus_Sentinel-1B_satellite

Phase-unwrapped interferogram stacks (SAR pairs) were generated using the ASF's HyP3 SAR processing algorithm⁸. A 20x4 look and adaptive phase filter of 0.6 were selected to reduce computational load during time-series analysis and enhance noise reduction. The 20x4 look denotes the pixel density and was selected for noise reduction. The adaptive phase filter reduces phase noise in the wrapped and unwrapped interferograms. A water mask was applied to minimize error during phase unwrapping of the interferograms given the potential for standing water within areas of Death Valley during the period of analysis. In addition to the interferogram stacks, a DEM and look vectors were produced as auxiliary products.

Small Baseline (SBAS) InSAR Time Series Analysis

InSAR time-series analysis and generation of average velocity estimates were performed using the ASF *OpenSAR Lab* run through *JupyterHub* and the University of Miami (SBAS) InSAR time series analysis workflow and software *MintPy* (Yunjun et al., 2019). This methodology uses weighted least squares inversion and is optimized for the generation of surface displacement time series. The workflow consists of the following steps:

(1) Load stack of phase unwrapped interferograms:

Unwrapped interferogram stacks, DEM's, azimuth angle maps, and incidence angle maps were directly loaded from the ASF HyP3 project folder. Interferogram stacks were subset and aligned to maximum extent of the area of interest – Death Valley.

(2) Coherence based network modification:

Interferograms with low percentage of high coherence pixels due to unwrapping errors

⁸ https://hyp3-docs.asf.alaska.edu/guides/insar_product_guide/

are identified and excluded. This coherence filter is critical to ensuring final velocity estimates and surface deformation represent areas of high coherence.

(3) Selection of reference point:

A random pixel was randomly selected with the following criteria to ensure a stable reference point to compare phase differences of the interferograms. The point was selected based on the following criteria: coherence > 0.85 ; minimal streaks caused by atmospheric turbulence; and elevation matching the designated area of interest.

(4) Network Inversion:

The network of differential unwrapped interferograms is inverted to estimate the unwrapped phase with respect to reference acquisition date of 12/30/2018. A temporal coherence mask (0.7) is generated to isolate pixels with reliable time series estimates. The water mask filters out pixels identified within standing water. A time series is generated representing distance change from radar to target.

(5) Tropospheric propagation delay correction:

Tropospheric delay is caused by variability in atmospheric moisture and can introduce error in the displacement measurements. This was corrected by incorporating atmospheric re-analysis data of geopotential, temperature, specific humidity, and pressure from the ECMWF ERA5 global atmospheric model are used to estimate hydrostatic and wet delay of the radar pulses to the target.

(6) Topographic residual DEM correction:

This correction was applied to correct topographic residuals resulting from errors in the DEM's used to generate the time series of interferograms. This involves estimating the topographic phase error from the time series of interferograms and adjusting the interferometric phase for each pixel to account for this error. This increases the accuracy of the final displacement estimates.

(7) Calculation of residual phase time series:

The root mean square (RMS) of the residual phase for each SAR acquisition date is calculated relative to a reference date with the minimum RMS value. This process refines the InSAR analysis by removing spatial errors and outliers, improving interpretability of the displacement measurements. The reference date selected was 12/1/2020 with RMS=0.0032.

(8) Average velocity estimation:

Ground deformation caused by many geophysical processes can generally be approximated as linear (Simons, 2015) and therefore the average velocity (rate of change of displacement) is estimated as the slope of the best fitting line to the displacement time series for each pixel.

Error Analysis

Uncertainty was evaluated by assessing the quality of the inversion of the interferogram stack and the accuracy of separating ground displacement from other components of the InSAR data. The following describes the methodology used to assess signal vs. noise in the analysis.

(1) Inversion quality:

The primary sources of noise during time series inversion are decorrelation, phase unwrapping and the inconsistency of triplets of interferograms. A triplet of interferograms is the process of evaluating phase among 3 separate SAR acquisitions to compare inconsistencies related to decorrelation, phase unwrapping errors, and atmospheric delays. The temporal average of spatial coherence and temporal coherence (threshold=0.7) of the entire interferogram stack was computed to identify erroneous pixels after time series inversion.

(2) Velocity error analysis:

The error long-term average velocity estimate from 2018-2023 was computed as a goodness of fit parameter.

The final output of the *MintPy* time series analysis consisted of temporal coherence, average spatial coherence, average velocity, and phase wrapped and unwrapped displacement GEOTIFF files which represent the relative displacement to the initial date in the series 12/30/2018. A total of 222 displacement TIFF files were compiled and used in the subsequent PCA deformation time series analysis.

2.3 Time Mode (T-Mode) Principal Component Analysis (TPCA)

Principal component analysis (PCA) is a statistical method that simplifies complex, high-dimensional data while retaining trends and patterns (Tabachnick et al., 2001). PCA was selected as the method of time-series analysis of the displacement GEOTIFF files for this study because it is well suited for exploratory analyses of spatial and temporal patterns of deformation without prior understanding of system dynamics (Chaussard, 2014). Principal

components (PC), also commonly referred to as empirical orthogonal functions, represent linear transformations of a set of correlated variables into a smaller set of uncorrelated (orthogonal) variables that captures most of the variability inherent in the untransformed data. T-mode PCA was selected for this analysis because it is ideal for evaluating time series data where the interest is understanding how patterns evolve over time across different locations, as opposed to S-mode which is useful for understanding relationships between variables (Richman, 1986). The 222 relative displacement GEOTIFF files produced from step 10 of the *MintPy* workflow were processed into a single data array ($X(m,n)$ matrix) consisting of 222 columns (time) representing a time step (SAR acquisition) and 748,904 rows, representing displacement values for each pixel in the area of interest. The T-PCA analysis was performed using the python machine learning library *scikit-learn*. To handle missing data from each displacement GEOTIFF, a mean imputation function was computed prior to the T-PCA analysis. The conceptual diagram of this workflow is described by Figure 3. A column chart (scree plot) representing the percentage of variance explained by the first 10 principal components was evaluated and the first 4 (PC) were selected for further analysis using the ‘rule of thumb’ method (North et al., 1982). Time series of eigenvectors or coefficients (loadings) were generated for these top 4 (PC). The eigenvector time series represent how the data’s projection onto the principal component changes over time. In addition to eigenvector time series, PC score maps were generated which are a spatial representation of the scores of a particular principal component for an area averaged over time. The PC score maps are useful because they show areas with similar behavior over time according to the specific PC.

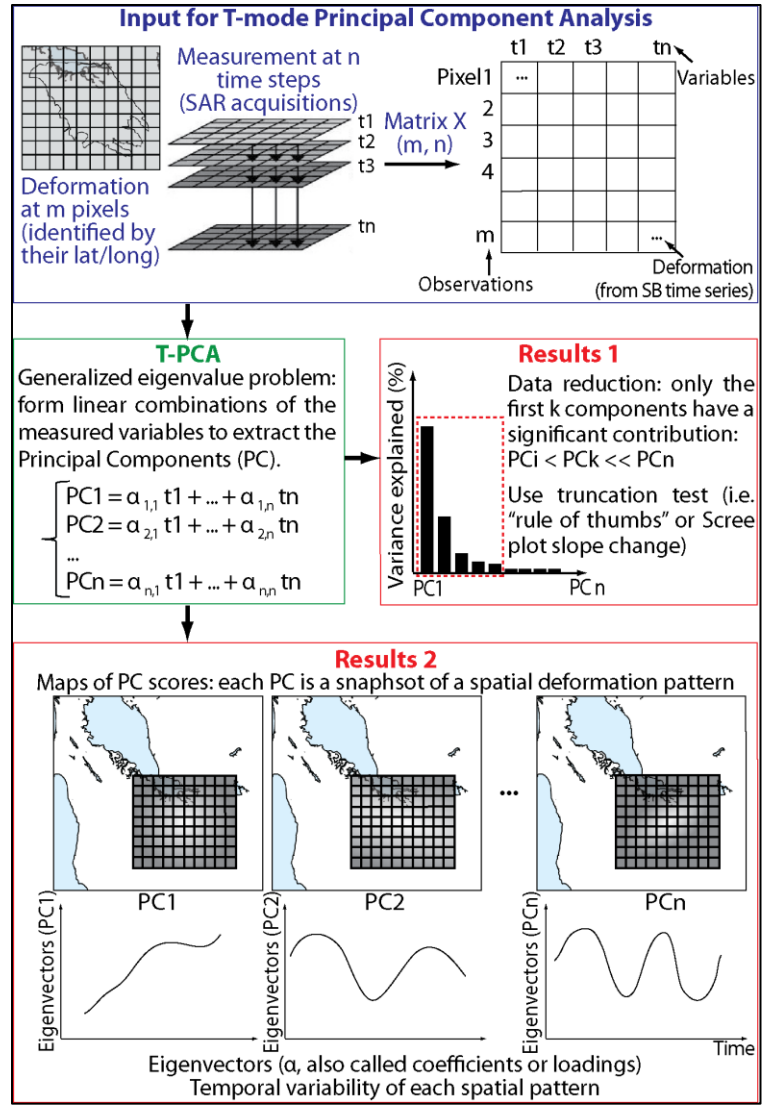


Figure 3: T-mode PCA analysis workflow for InSAR data. Figure from (Chaussard et al., 2014).

3. RESULTS

Average daily temperature of Death Valley has increased ~ 2 degrees Fahrenheit from the baseline period to the comparison period. (Figure 4a). This observation aligns with the generalized conceptual model of an average increase in global mean surface temperature. From 1961 to 1991 (base period) there were 10,454 days without recorded precipitation and 503 days

with recorded precipitation from a sample of n=10,957 days for that period; 95.7% of days had no precipitation and 4.3% recorded precipitation. From 1991 to 2023 (comparison period) there were 11,435 days without recorded precipitation and 519 days with recorded precipitation from a sample of n=11,954 days implying 95.7% of days had no precipitation and 4.3% recorded precipitation. There was no change in the relative number of dry vs. wet days across the two periods. The following table describes the number of daily events in a frequency percentile for each analysis period (Figure 4b):

Table 2. The number of daily events in a frequency percentile for each analysis period.

Percentiles of Daily Precipitation Events	Number of Days in Baseline Period (1961-1991)	Number of Days in Comparison Period (1991-2023)
99th	3	8
98th	7	3
97th	5	4
95th	8	14
90th	25	26

Figure 4c indicates that the magnitude of extreme events has increased from the comparison period to the base period. However, events with <2.5% exceedance probability remained the same across both periods.

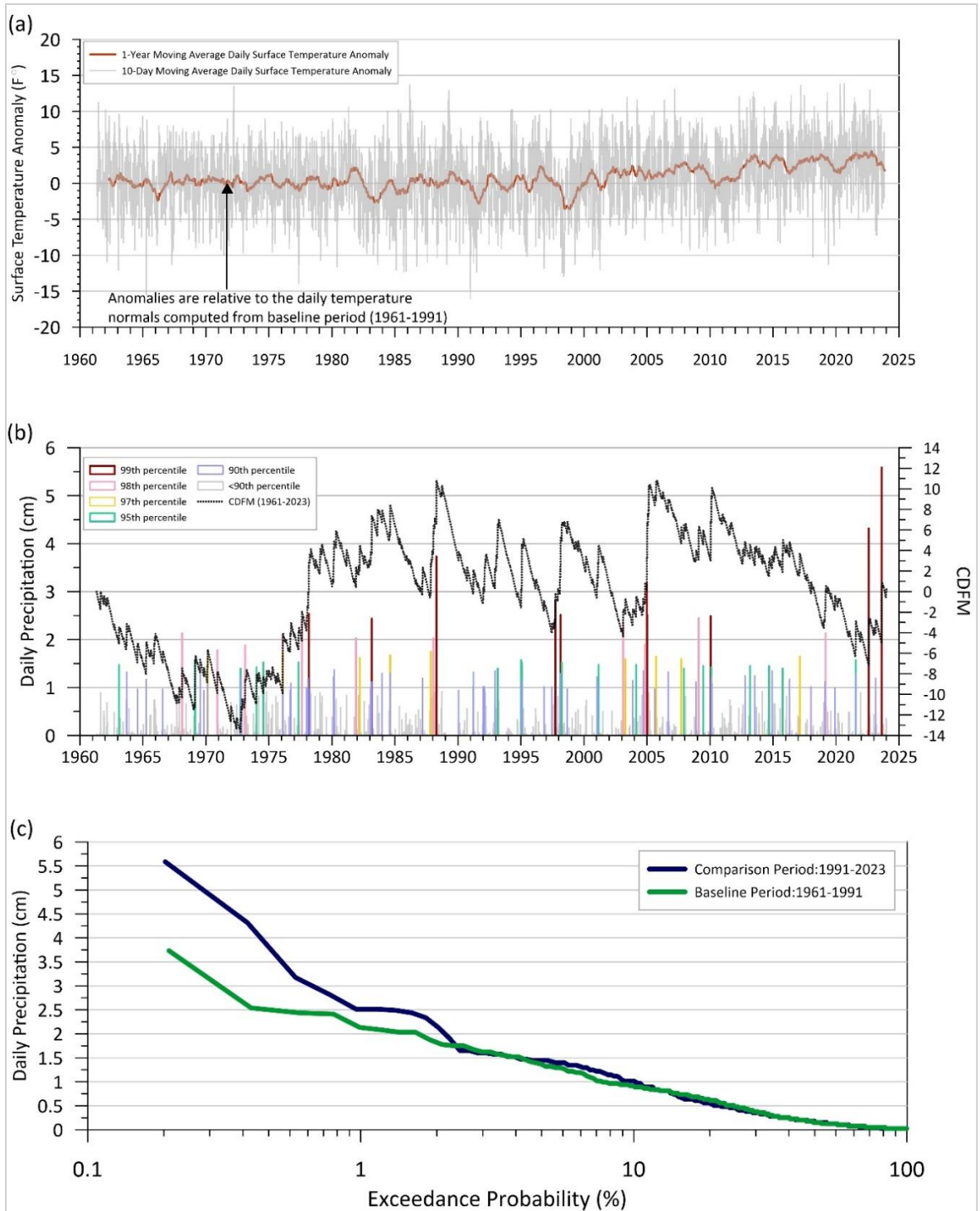


Figure 4: Death Valley: (a) Land surface daily temperature anomalies for the period (1961-2023). The anomalies are computed relative to the baseline period of 1961-1991 and indicate a general trend toward higher temperatures. (b) daily precipitation frequency percentiles and cumulative difference from long-term mean CDFM (1961-2023) (c) exceedance probabilities of daily precipitation events across the baseline and comparison period.

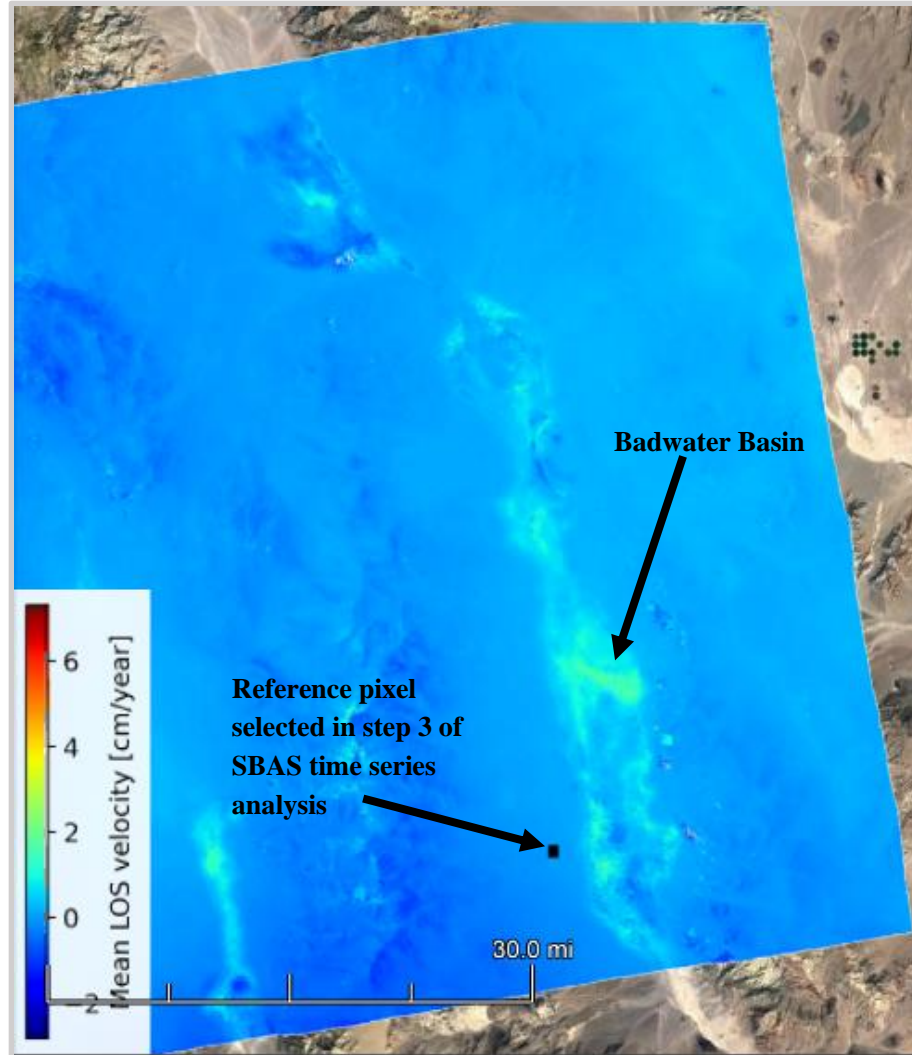


Figure 5: Mean line of sight velocity (LOS) of Death Valley from December 30, 2018 to December 10, 2023.

Death Valley experienced a prolonged dry period from 2015 to 2023 as indicated by the CDFM corroborated with GRACE water equivalent thickness (cm) punctuated by wet months in 2018, 2021, 2022 and 2023 (Figure 6a). The InSAR time series analysis indicates that the land surface elevation in many parts of Death Valley experienced an average vertical displacement (uplift) of ~1.5 to 2 cm (Figure 5). The most pronounced uplift occurred in Badwater Basin with ~3 cm of vertical displacement recorded. This uplift coincides with the wet months beginning in 2018.

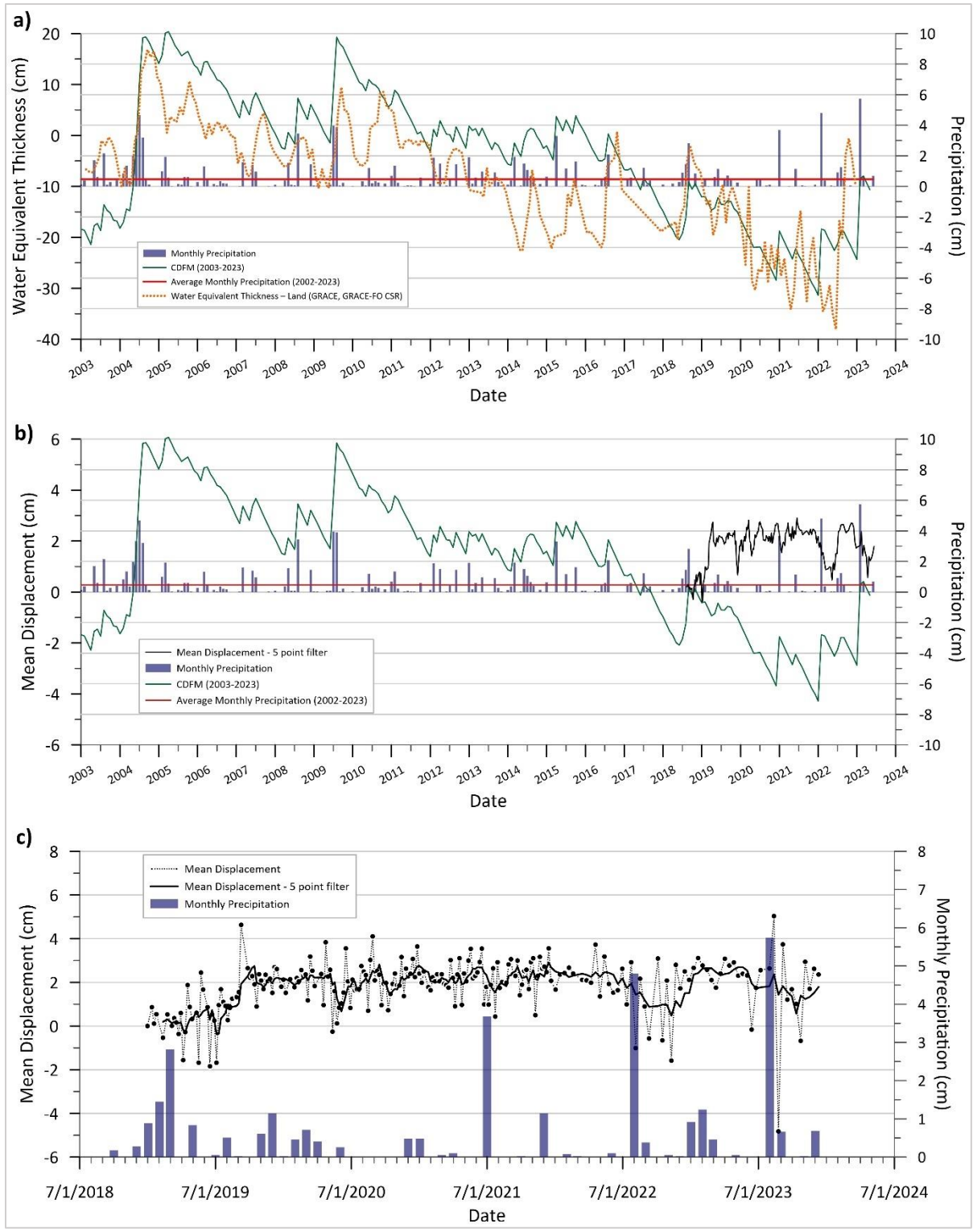


Figure 6: (a) CDFM, GRACE water equivalent thickness, and monthly precipitation; (b) mean-displacement in Death Valley, CDFM and monthly precipitation from 2003-2023; (c) mean surface displacement and filtered mean surface displacement vs. monthly precipitation.

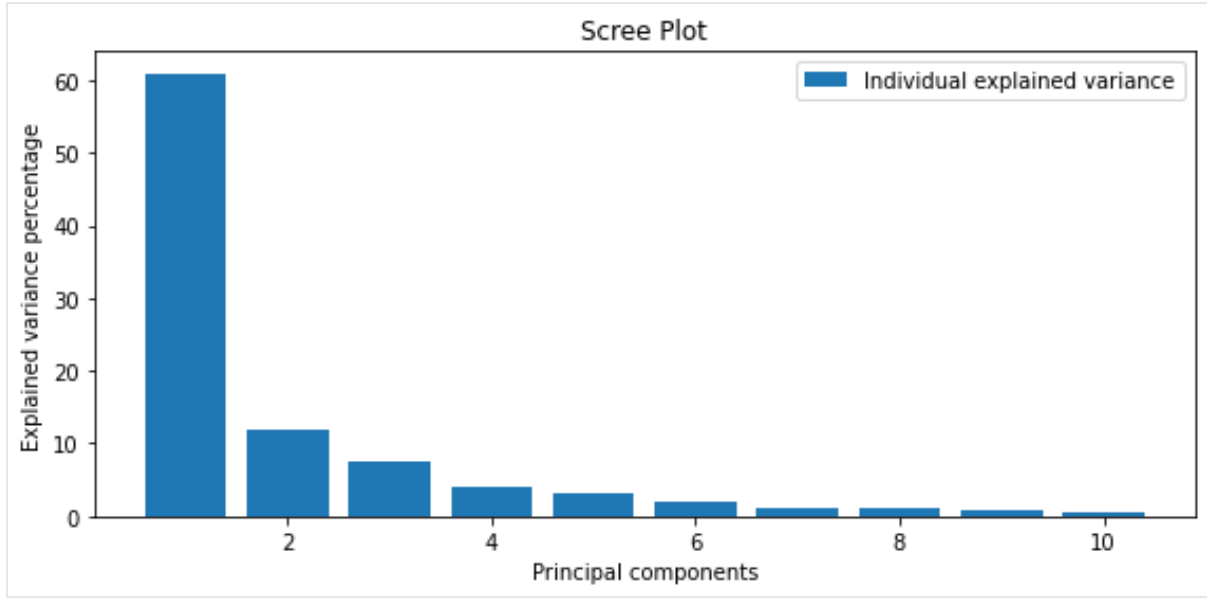


Figure 7: Explained variance of the first 10 principal components from the T-PCA analysis.

The results of the T-PCA analysis indicate that PC1 is consistent with the mean displacement in Death Valley. It is likely that the signal portrayed by the PC1 eigenvector relates to the physical process of vertical displacement resulting from precipitation. The three consecutive months of precipitation at the beginning of the TPCA analysis period (2018-2023) are likely contributing to the uplift. This is corroborated by the sharp increase in water equivalent thickness in 2018 (Figure 6a). The PC2 eigenvector represents the dominant mode corresponding to deformation responses to specific months of high precipitation. Across the 4 PC eigenvectors there is an increase in amplitude corresponding to the high precipitation months in 2021, 2022, and 2023. In addition, there is a consistent strong signal of explained variance across PC1, PC2, PC3, and PC4 in Badwater Basin.

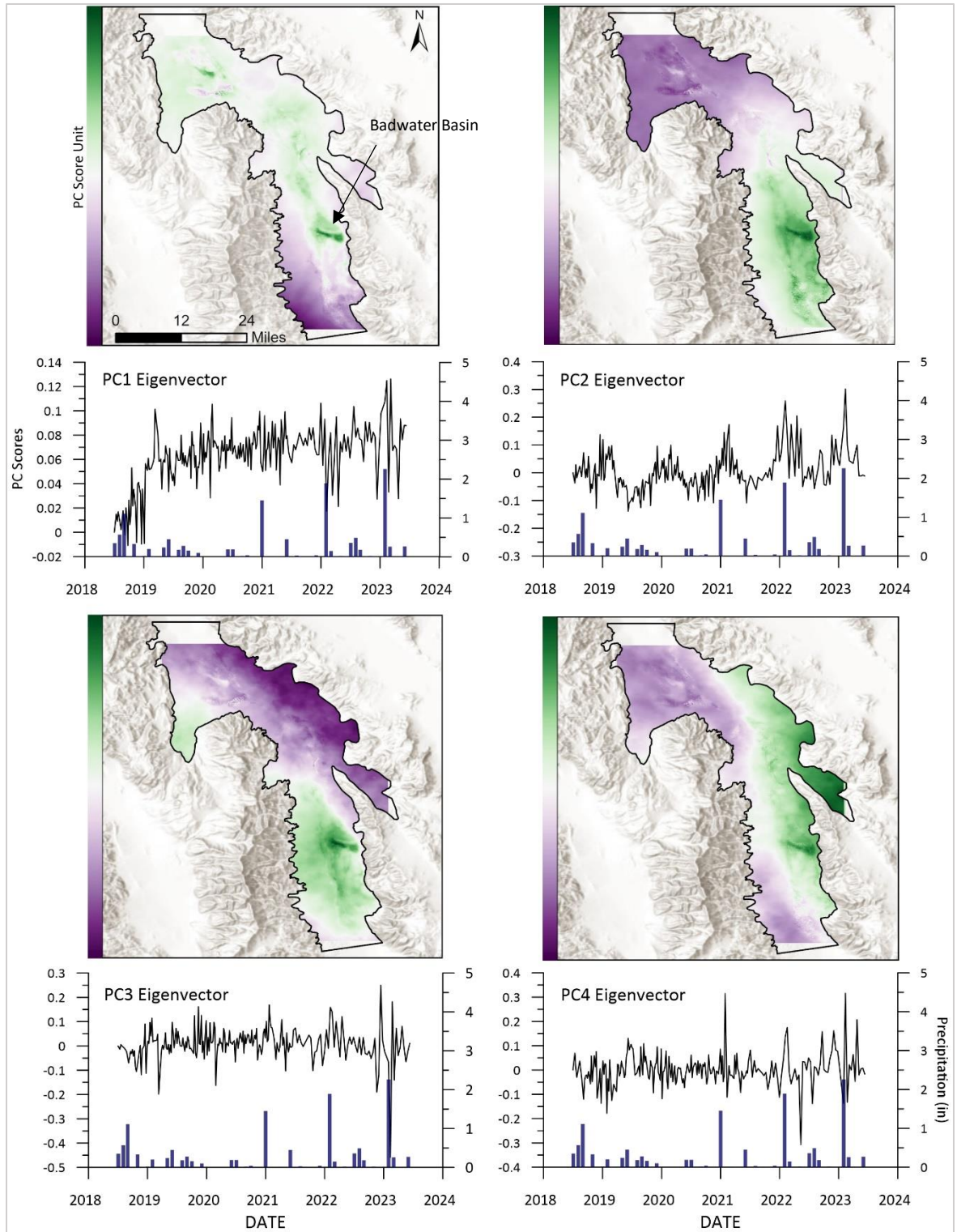


Figure 8: Results of TPCA analysis and corresponding eigenvector time series and PC score maps for PC1, PC2, PC3, and PC4.

4. DISCUSSION

Uplift has occurred in Death Valley over the period 2018-2023. It is likely that a combination of consecutive months of above average precipitation in 2018 and 3 anomalous daily events (98th and 99th percentile) contributed to enhanced groundwater recharge, inducing upward vertical surface deformation. The bajada and alluvial fans on either side of Death Valley likely act as conduits for focused intense groundwater recharge. While these focused pulses of recharge are a likely contributing factor to increased poroelastic pressure in the compressible sediments at depth (clay formations), it is uncertain to what degree these deeper processes contribute to observed uplift. Death Valley is the regional base level, and these pulsed events may be contributing to pressure differentials across the regional groundwater flow system. The pressure differentials may cause groundwater to upwell and induce a decrease in vertical effective stress resulting in uplift. Another likely contributing factor to vertical surface deformation is the expansion of the halite of the salt pan from wetting. This would explain the enhanced uplift localized in Badwater Basin, but is likely not contributing to average upward vertical displacement across the valley due to the heterogenous distribution and composition of surficial sediments. Analysis of land surface mineral composition using electromagnetic resistivity or SAR data could be used to evaluate the potential spatial correlation between surface composition of the land surface and patterns of deformation.

The results of this study provide a quantitative link between surface displacement and recharge. A more robust analysis incorporating other data sources recorded at extended temporal intervals is needed to allow for definitive statements relating groundwater fluxes to extreme precipitation events.

5. CONCLUSIONS

Spatiotemporal and cross-correlation analysis of deformation patterns using gridded precipitation data could be explored to determine the potential lag between precipitation and deformation data, which would expand upon the results of this study. A more concise understanding of the effect of long-term fluctuations of extreme precipitation events on groundwater fluxes requires a more in-depth precipitation frequency analysis quantifying the probability distribution functions of precipitation magnitude and frequency over the period of analysis. The results of this study could contribute to calibration efforts and be tested against aquifer properties estimated by the Death Valley Regional Groundwater Flow System Transient Model (DVRFS) produced by the USGS.

This work provides a novel case study that will contribute to the understanding of groundwater fluxes in a warming world and provides a benchmark for future efforts to understand the effects of precipitation variability on groundwater recharge in arid environments.

REFERENCES

- Abbott, Benjamin W., Kevin Bishop, Jay P. Zarnetske, Camille Minaudo, F. S. Chapin, Stefan Krause, David M. Hannah, et al. (2019). “Human Domination of the Global Water Cycle Absent from Depictions and Perceptions.” *Nature Geoscience* 12, no. 7: 533–40. <https://doi.org/10.1038/s41561-019-0374-y>.
- Adloff, Markus, Michael Bliss Singer, David A. MacLeod, Katerina Michaelides, Nooshin Mehrnegar, Eleanor Hansford, Chris Funk, and Daniel Mitchell. (2022). “Sustained Water Storage in Horn of Africa Drylands Dominated by Seasonal Rainfall Extremes.” *Geophysical Research Letters* 49, no. 21: e2022GL099299. <https://doi.org/10.1029/2022GL099299>.
- Ahamed, Aakash, Rosemary Knight, Sarfaraz Alam, Rich Pauloo, and Forrest Melton. (2022). “Assessing the Utility of Remote Sensing Data to Accurately Estimate Changes in Groundwater Storage.” *Science of The Total Environment* 807: 150635. <https://doi.org/10.1016/j.scitotenv.2021.150635>.
- Amelung, Falk, Devin L. Galloway, John W. Bell, Howard A. Zebker, and Randell J. Laczniaik. (1999). “Sensing the Ups and Downs of Las Vegas: InSAR Reveals Structural Control of Land Subsidence and Aquifer-System Deformation.” *Geology* 27, no. 6: 483–86. [https://doi.org/10.1130/0091-7613\(1999\)027<0483:STUADO>2.3.CO;2](https://doi.org/10.1130/0091-7613(1999)027<0483:STUADO>2.3.CO;2).
- Bedinger, M. S., and J. R. Harrill. 2012. Groundwater geology and hydrology of Death Valley National Park, California and Nevada. Natural Resource Technical Report NPS/NRSS/WRD/NRTR—2012/652. National Park Service, Fort Collins, Colorado.
- Belcher, W.R., Sweetkind, D.S., Faunt, C.C., Pavelko, M.T., and Hill, M.C. (2017). An update of the Death Valley regional groundwater flow system transient model, Nevada and California: U.S. Geological Survey Scientific Investigations Report 2016-5150, 74 p., 1 pl. <https://doi.org/10.3133/sir20165150>
- Berardino, Paolo, Gianfranco Fornaro, Riccardo Lanari, and Eugenio Sansosti. (2002). “A New Algorithm for Surface Deformation Monitoring Based on Small Baseline Differential SAR Interferograms.” *Geoscience and Remote Sensing, IEEE Transactions On* 40: 2375–83. <https://doi.org/10.1109/TGRS.2002.803792>.
- Bierkens, Marc F. P., and Yoshihide Wada. (2019). “Non-Renewable Groundwater Use and Groundwater Depletion: A Review.” *Environmental Research Letters* 14, no. 6: 063002. <https://doi.org/10.1088/1748-9326/ab1a5f>.

Castellazzi, Pascal, Richard Martel, Devin L. Galloway, Laurent Longuevergne, and Alfonso Rivera. (2016). “Assessing Groundwater Depletion and Dynamics Using GRACE and InSAR: Potential and Limitations.” *Groundwater* 54, no. 6: 768–80.

<https://doi.org/10.1111/gwat.12453>.

Chaussard, E., R. Bürgmann, M. Shirzaei, E. J. Fielding, and B. Baker. (2014).

“Predictability of Hydraulic Head Changes and Characterization of Aquifer-System and Fault Properties from InSAR-Derived Ground Deformation.” *Journal of Geophysical Research: Solid Earth* 119, no. 8: 6572–90. <https://doi.org/10.1002/2014JB011266>.

Cuthbert, Mark O., Richard G. Taylor, Guillaume Favreau, Martin C. Todd, Mohammad Shamsudduha, Karen G. Villholth, Alan M. MacDonald, et al. (2019). “Observed Controls on Resilience of Groundwater to Climate Variability in Sub-Saharan Africa.” *Nature* 572, no. 7768: 230–34. <https://doi.org/10.1038/s41586-019-1441-7>.

Domenic, P.A., Schwartz, F.W. (1998). *Physical and Chemical Hydrogeology*. 2nd. ed. John Wiley & Sons, New York.

Durack, Paul J. (2015). “Ocean Salinity and the Global Water Cycle.” *Oceanography* 28, no. 1: 20–31.

Ferretti, Alessandro, Andrea Monti-Guarnieri, Claudio Prati, Fabio Rocca, and Didier Massonet. (2007). “InSAR Principles - Guidelines for SAR Interferometry Processing and Interpretation.” *ESA Training Manual* 19.

Fetter, C.W. (2001) *Applied Hydrogeology*. 4th Edition, Prentice Hall, Upper Saddle River.

Fischer, E. M., and R. Knutti. (2016). “Observed Heavy Precipitation Increase Confirms Theory and Early Models.” *Nature Climate Change* 6, no. 11: 986–91.

<https://doi.org/10.1038/nclimate3110>.

Fermi, E. (1936). *Thermodynamics*. Dover Publications, New York.

Freeze, R.A., and Cherry, J.A. (1979). *Groundwater*: Englewood Cliffs, NJ, Prentice-Hall, 604.

Galloway, Devin L., and Jörn Hoffmann. (2007). “The Application of Satellite Differential SAR Interferometry-Derived Ground Displacements in Hydrogeology.” *Hydrogeology Journal* 15, no. 1: 133–54. <https://doi.org/10.1007/s10040-006-0121-5>.

Glazner, Allen, A.G. Sylvester, and Robert Sharp. (2022) *Geology Underfoot in Death Valley and Eastern California, 2nd Edition*.

- Goldstein, Richard M., Hermann Engelhardt, Barclay Kamb, and Richard M. Frolich. (1993). “Satellite Radar Interferometry for Monitoring Ice Sheet Motion: Application to an Antarctic Ice Stream.” *Science* 262, no. 5139: 1525–30. <https://doi.org/10.1126/science.262.5139.1525>.
- Hunt, Charles Butler, and Don R. Mabey. (1966). “Stratigraphy and Structure, Death Valley, California.” Report. Professional Paper. USGS Publications Warehouse. <https://doi.org/10.3133/pp494A>.
- Hunt, Charles Butler, T. W. Robinson, W.A. Bowles, and A.L. Washburn. (1966). “Hydrologic Basin, Death Valley, California.” Report. Professional Paper. USGS Publications Warehouse. <https://doi.org/10.3133/pp494B>.
- Ingebritsen, S., Sanford, W., Neuzil, C. (2006). *Groundwater in Geologic Processes*. 2nd ed., Cambridge University Press, Cambridge, UK.
- Jasechko, Scott. (2019). “Global Isotope Hydrogeology—Review.” *Reviews of Geophysics* 57, no. 3: 835–965. <https://doi.org/10.1029/2018RG000627>.
- Jasechko, Scott, and Debra Perrone. (2021). “Global Groundwater Wells at Risk of Running Dry.” *Science* 372, no. 6540: 418–21. <https://doi.org/10.1126/science.abc2755>.
- Jasechko, Scott, Hansjörg Seybold, Debra Perrone, Ying Fan, Mohammad Shamsudduha, Richard G. Taylor, Othman Fallatah, and James W. Kirchner. (2024). “Rapid Groundwater Decline and Some Cases of Recovery in Aquifers Globally.” *Nature* 625, no. 7996: 715–21. <https://doi.org/10.1038/s41586-023-06879-8>.
- Lees, Matthew, Rosemary Knight, and Ryan Smith. (2021). *Modeling 65 Years of Land Subsidence in California’s San Joaquin Valley*. <https://doi.org/10.21203/rs.3.rs-609832/v1>.
- Levy, Morgan C., Wesley R. Neely, Adrian A. Borsa, and Jennifer A. Burney. (2020). “Fine-Scale Spatiotemporal Variation in Subsidence across California’s San Joaquin Valley Explained by Groundwater Demand.” *Environmental Research Letters* 15, no. 10: 104083. <https://doi.org/10.1088/1748-9326/abb55c>.
- Loáiciga, H.A. (2009). “Derivation approaches for the Theis equation”. *Groundwater*, 47(4), 1-4. <https://doi.org/10.1111/j.1745-6584.2009.00568.x>
- Loáiciga, Hugo A., Thomas J. Pingel, and Elizabeth S. Garcia. (2012). “Sea Water Intrusion by Sea-Level Rise: Scenarios for the 21st Century.” *Groundwater* 50, no. 1 (2012): 37–47. <https://doi.org/10.1111/j.1745-6584.2011.00800.x>.

- Loáiciga, Hugo A. (2013). “Consolidation Settlement in Aquifers Caused by Pumping.” *Journal of Geotechnical and Geoenvironmental Engineering* 139, no. 7: 1191–1204. [https://doi.org/10.1061/\(ASCE\)GT.1943-5606.0000836](https://doi.org/10.1061/(ASCE)GT.1943-5606.0000836).
- Loáiciga, Hugo A. (2017). “The Safe Yield and Climatic Variability: Implications for Groundwater Management.” *Groundwater* 55, no. 3: 334–45. <https://doi.org/10.1111/gwat.12481>.
- Loaiciga, H.A., Doh, R. (2024). “Groundwater for humans and the environment: a globally threatened resource”. *Groundwater*. <https://doi.org/10.1111/gwat.13376>
- Lohman, Stanley William. (1972) “Ground-Water Hydraulics.” *Professional Paper*. U.S. Geological Survey. <https://doi.org/10.3133/pp708>.
- Meinshausen, Malte, Elisabeth Vogel, Alexander Nauels, Katja Lorbacher, Nicolai Meinshausen, David M. Etheridge, Paul J. Fraser, et al. (2017). “Historical Greenhouse Gas Concentrations for Climate Modelling (CMIP6).” *Geoscientific Model Development* 10, no. 5: 2057–2116. <https://doi.org/10.5194/gmd-10-2057-2017>.
- Myhre, G., K. Alterskjær, C. W. Stjern, Ø Hodnebrog, L. Marelle, B. H. Samset, J. Sillmann, et al. (2019). “Frequency of Extreme Precipitation Increases Extensively with Event Rareness under Global Warming.” *Scientific Reports* 9, no. 1: 16063. <https://doi.org/10.1038/s41598-019-52277-4>.
- Neely, Wesley R., Adrian A. Borsa, Jennifer A. Burney, Morgan C. Levy, Francesca Silverii, and Michelle Sneed. (2021). “Characterization of Groundwater Recharge and Flow in California’s San Joaquin Valley From InSAR-Observed Surface Deformation.” *Water Resources Research* 57, no. 4: e2020WR028451. <https://doi.org/10.1029/2020WR028451>.
- North, Gerald R., Thomas L. Bell, Robert F. Cahalan, and Fanthune J. Moeng. (1982). “Sampling Errors in the Estimation of Empirical Orthogonal Functions.” *Monthly Weather Review* 110, no. 7: 699–706. [https://doi.org/10.1175/1520-0493\(1982\)110<0699:SEITEO>2.0.CO;2](https://doi.org/10.1175/1520-0493(1982)110<0699:SEITEO>2.0.CO;2).
- O’Gorman, Paul A., Richard P. Allan, Michael P. Byrne, and Michael Previdi. (2012). “Energetic Constraints on Precipitation Under Climate Change.” *Surveys in Geophysics* 33, no. 3: 585–608. <https://doi.org/10.1007/s10712-011-9159-6>.
- Pendergrass, Angeline G. (2018). “What Precipitation Is Extreme?” *Science* 360, no. 6393: 1072–73. <https://doi.org/10.1126/science.aat1871>.

- Riel, Bryan, Mark Simons, Daniel Ponti, Piyush Agram, and Romain Jolivet. (2018). “Quantifying Ground Deformation in the Los Angeles and Santa Ana Coastal Basins Due to Groundwater Withdrawal.” *Water Resources Research* 54, no. 5: 3557–82. <https://doi.org/10.1029/2017WR021978>.
- Richman, Michael B. (1986). “Rotation of Principal Components.” *Journal of Climatology* 6, no. 3: 293–335. <https://doi.org/10.1002/joc.3370060305>.
- Save, Himanshu, Srinivas Bettadpur, and Byron D. Tapley. (2016). “High-Resolution CSR GRACE RL05 Mascons.” *Journal of Geophysical Research: Solid Earth* 121, no. 10: 7547–69. <https://doi.org/10.1002/2016JB013007>.
- Scanlon, B. R., L. Longuevergne, and D. Long. (2012). “Ground Referencing GRACE Satellite Estimates of Groundwater Storage Changes in the California Central Valley, USA.” *Water Resources Research* 48, no. 4. <https://doi.org/10.1029/2011WR011312>.
- Schär, Christoph, Nikolina Ban, Erich M. Fischer, Jan Rajczak, Jürg Schmidli, Christoph Frei, Filippo Giorgi, et al. (2016). “Percentile Indices for Assessing Changes in Heavy Precipitation Events.” *Climatic Change* 137, no. 1: 201–16. <https://doi.org/10.1007/s10584-016-1669-2>.
- Sentinel-1: ESA’s Radar Observatory Mission for GMES Operational Services (ESA SP-1322/1, March 2012) https://sentinel.esa.int/documents/247904/349449/s1_sp-1322_1.pdf
- Seo, Ki-Weon, Dongryeol Ryu, Jooyoung Eom, Taewhan Jeon, Jae-Seung Kim, Kookhyoun Youm, Jianli Chen, and Clark R. Wilson. (2023). “Drift of Earth’s Pole Confirms Groundwater Depletion as a Significant Contributor to Global Sea Level Rise 1993–2010.” *Geophysical Research Letters* 50, no. 12: e2023GL103509. <https://doi.org/10.1029/2023GL103509>.
- Simons, M., and P. A. Rosen. (2007). “Interferometric Synthetic Aperture Radar Geodesy”. In *Treatise on Geophysics - Geodesy*, 391–446. Amsterdam: Elsevier.
- Simpson, Isla R., Karen A. McKinnon, Daniel Kennedy, David M. Lawrence, Flavio Lehner, and Richard Seager. (2024). “Observed Humidity Trends in Dry Regions Contradict Climate Models.” *Proceedings of the National Academy of Sciences* 121, no. 1: e2302480120. <https://doi.org/10.1073/pnas.2302480120>.
- Smith, Laurence C. (2002). “Emerging Applications of Interferometric Synthetic Aperture Radar (InSAR) in Geomorphology and Hydrology.” *Annals of the Association of American Geographers* 92, no. 3: 385–98.

- Smith, R., and R. Knight. (2019). "Modeling Land Subsidence Using InSAR and Airborne Electromagnetic Data." *Water Resources Research* 55, no. 4: 2801–19. <https://doi.org/10.1029/2018WR024185>.
- Tabachnick, B. G., L. S. Fidell, and S. J. Osterlind (2001), *Using Multivariate Statistics*, 3rd ed., Harper Collins, New York.
- Tapley, B. D., S. Bettadpur, M. Watkins, and C. Reigber. (2004). "The Gravity Recovery and Climate Experiment: Mission Overview and Early Results." *Geophysical Research Letters* 31, no. 9. <https://doi.org/10.1029/2004GL019920>.
- Taylor, Charles J., and William M. Alley. (2001). "Ground-Water-Level Monitoring and the Importance of Long-Term Water-Level Data." *Circular*. <https://doi.org/10.3133/cir1217>.
- (a) Taylor, Richard G., Bridget Scanlon, Petra Döll, Matt Rodell, Rens van Beek, Yoshihide Wada, Laurent Longuevergne, et al. (2013). "Ground Water and Climate Change." *Nature Climate Change* 3, no. 4: 322–29. <https://doi.org/10.1038/nclimate1744>.
- (b) Taylor, Richard G., Martin C. Todd, Lister Kongola, Louise Maurice, Emmanuel Nahozya, Hosea Sanga, and Alan M. MacDonald. (2013). "Evidence of the Dependence of Groundwater Resources on Extreme Rainfall in East Africa." *Nature Climate Change* 3, no. 4: 374–78. <https://doi.org/10.1038/nclimate1731>.
- Terzaghi, K. (1925). Principles of soil mechanics: IV. Settlement and consolidation of clay, *Erdbaummechanik*, 95(3), 874–878
- Theis, C. V. (1935). "The relation between the lowering of the piezometric surface and rate and duration of discharge of a well using ground water storage." *Trans. Am. Geophys. Union*, 16, 519–524
- Todd, D.K. (1980). *Groundwater Hydrology*, 2nd ed., John Wiley & Sons, New York, 535p.
- United Nations, The United Nations World Water Development Report 2022: Groundwater: Making the invisible visible. UNESCO, Paris.
- Vasco, Donald W., Kyra H. Kim, Tom G. Farr, J. T. Reager, David Bekaert, Simran S. Sangha, Jonny Rutqvist, and Hiroko K. Beaudoin. (2022). "Using Sentinel-1 and GRACE Satellite Data to Monitor the Hydrological Variations within the Tulare Basin, California." *Scientific Reports* 12, no. 1: 3867. <https://doi.org/10.1038/s41598-022-07650-1>.
- Wildermuth Environmental, Inc. [WEI] (2019). Optimum Basin Management Program 2018 State of the Basin Atlas. Prepared for the Chino Basin Watermaster.

Yunjun, Zhang, Heresh Fattahi, and Falk Amelung. (2019). “Small Baseline InSAR Time Series Analysis: Unwrapping Error Correction and Noise Reduction.” *Computers & Geosciences* 133: 104331. <https://doi.org/10.1016/j.cageo.2019.104331>.